THE JOURNAL OF PHYSICAL CHEMISTRY C

Article

pubs.acs.org/JPCC

Reactivity and Morphology of Oxygen-Modified Au Surfaces

Ashleigh E. Baber,[†] Daniel Torres,[‡] Kathrin Müller,[‡,§] Marcelo Nazzarro,[∥] Ping Liu,[‡] David E. Starr,[‡] and Dario J. Stacchiola*[,†]

[†]Chemistry Department and [‡]Center for Functional Nanomaterials, Brookhaven National Laboratory, Upton, New York 11973, United States

[∥]Laboratorio de Ciencias de Superficies, Dpto de Física, UNSL and INFAP, CONICET, San Luis 5700, Argentina

[§]Zernike Institute for Advanced Materials, University of Groningen, 9747 AG Groningen, The Netherlands

ABSTRACT: Inducing the adsorption of oxygen on gold surfaces transforms the inert metal into a surprisingly reactive material, which acts as a highly selective, low-temperature catalyst. The strong interaction of atomic oxygen with Au greatly affects the surface morphology by increasing the number of undercoordinated Au atoms and lifting the surface reconstruction. Through the combination of experimental and theoretical techniques, we have fully characterized an oxygen-modified Au(100) surface and determined the structure–reactivity relationship of O–Au species. Bulk-implanted oxygen does not affect the reactivity of Au surfaces and subsurface oxygen is found to be unstable. Oxygen stabilizes undercoordinated Au atoms on the surface and becomes highly active for oxidation reactions when adsorbed on unreconstructed Au(100) sites.

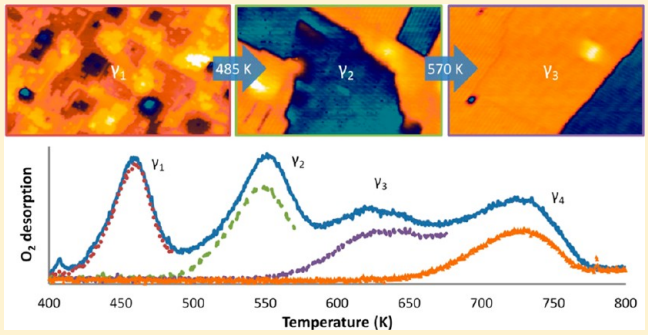

INTRODUCTION

The discovery of gold's surprising low-temperature activity[1] opened an entire field for Au-based catalysis studies.[2] Gold single crystals have been exploited to investigate and better understand the roots of the complex catalytic processes.[3−5] Although extended Au substrates are inert, they can be converted into very reactive surfaces by the adsorption of atomic oxygen. However, due to its large activation barrier on gold surfaces, oxygen dissociation must be induced to carry out experiments under ultrahigh vacuum (UHV) conditions.[4,6−10] Several commonly used methods for adsorbing atomic oxygen on gold include ozone exposure,[11] the reaction of preadsorbed H_2O and NO_2,[12,13] thermal dissociation of molecular oxygen over a hot filament,[14−16] exposure to an oxygen plasma,[17] oxygen-sputtering,[8,18] and electron-assisted activation of adsorbed molecular oxygen.[19] The adsorption of atomic oxygen causes structural changes on Au surfaces, resulting in surface morphologies with an increased number of undercoordinated Au atoms, which are associated with an increase in the catalytic activity of these surfaces.[10,19−25] In the case of oxygen-sputtering, modifying the substrate temperature, and the flux and energy of ions during the process allows control over the adsorbed oxygen phase on the Au surface. The resulting model catalytic system can be used to study the details of low-temperature oxidation reactions on Au.

Oxygen-sputtering is a convenient way to induce oxygen adsorption and provides the possibility of controlling the surface morphology and adsorption state of the oxygen. Previous temperature programmed desorption (TPD) studies of an O_2-sputtered Au(110)-1 × 2 system revealed the presence of four oxygen states (γ_1, γ_2, γ_3, γ_4) with desorption temperatures at 415, 545, 620, and 750 K, respectively.[8] It was found that sputtering at progressively higher ion energies (from 1 to 5 keV) increased the amount of oxygen in the higher temperature desorption states (γ_3, γ_4), assigned to oxygen implanted under the surface.[8] The γ_3 phase was speculated to reside in the subsurface region because it was not fully reactively consumed after CO exposure, while γ_4 was assigned to O deep in the bulk.[8] When a similar approach to dissociate oxygen on Au(111) was used, the γ_3 oxygen state was shown to have no effect on reactivity on Au(111) for styrene epoxidation, supporting the subsurface assignment.[26] The lower temperature desorption peaks, γ_1 and γ_2, were assigned to gold oxide and surface chemisorbed oxygen, respectively,[8] although it has since been suggested that these peaks represent two different surface oxygen species adsorbed on Au.[26] The oxygen present on Au(111) has been characterized by three species and correlated to CO reactivity, listed here from most to least reactive: chemisorbed oxygen, surface oxide, and bulk oxide.[27,28]

Herein, we report the oxygen species present on Au(100) after oxygen-sputtering using TPD, and compare our findings to those from Au(110)-1 × 2 and Au(111). We have used scanning tunneling microscopy (STM) to capture structural changes that accompany thermal treatments and oxygen

Received: June 10, 2012
Revised: August 3, 2012
Published: August 7, 2012

   dx.doi.org/10.1021/jp3056653 | J. Phys. Chem. C 2012, 116, 18292−18299

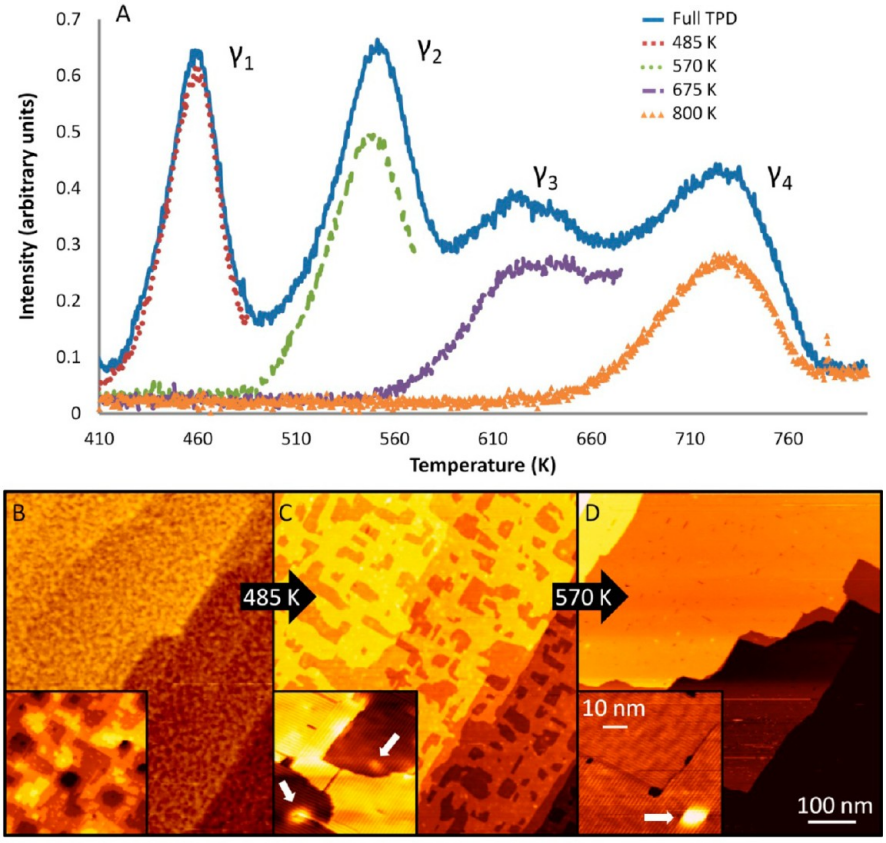

Figure 1. Sectional TPD spectra of an oxygen-sputtered Au(100) single crystal, with corresponding room temperature STM images of the thermally treated surface. (A) Full and partial TPDs. The temperatures in the legend represent the maximum annealing temperatures for the partial TPDs. (B) STM image (and inset) of the as-sputtered surface. Scanning conditions: −1.6 V, 0.4 nA; Inset: 0.9 V, 0.9 nA. (C) Surface morphology after annealing to 485 K, in which γ_1 has fully desorbed. The white arrows point to "blisters". Scanning conditions: 1.2 V, 1.2 nA. (D) STM image after annealing to 570 K (only γ_3, γ_4 present) showing that the surface has healed. Scanning conditions: 1.1 V, 1.2 nA; Inset: 1.1 V, 0.6 nA. The scale bars in D also correspond to the images in B and C.

removal, thereby shedding light on the nature of the oxygen phases present after sputtering, in particular the low-temperature oxygen desorption states (γ_1 and γ_2), which have previously been disputed. In addition to TPD and STM, we used X-ray photoelectron spectroscopy (XPS), CO reactivity studies, and density functional theory (DFT) to fully characterize the O/Au(100) system.

EXPERIMENTAL SECTION

All experiments were performed in an UHV stainless steel chamber with a variable-temperature RHK STM, Specs XPS, and TPD capabilities in the Proximal Probes Facility at the Center for Functional Nanomaterials at Brookhaven National Laboratory. The base pressure of the system is 2×10^{-10} Torr. For the TPD experiments, all reported temperatures are within ±5 K. XPS experiments were conducted using an Al Kα lab X-ray source. All STM images were recorded at room temperature with electrochemically etched and *in situ* sputtered tungsten tips. The samples were cleaned using standard procedures reported in the literature.[12] TPD studies were conducted with a differentially pumped nozzle several millimeters from the surface, with a heating rate of 100 K/min. The temperature was measured with a K-type thermocouple directly attached to the Au(100) single crystal. To obtain sectional TPD spectra (as seen in Figure 1A), the Au(100) sample was sputtered with oxygen ions and then annealed to sequentially higher temperatures while monitoring the desorption of O_2. Between each measurement, the sample was allowed to cool to <350 K. For the investigation of oxygen on Au(100), we aim to better understand the low-temperature desorption states of oxygen on the surface, rather than oxygen implanted into the bulk. Therefore, the studies shown below are conducted at the lowest limit of the sputtering ion energy: 0.5 keV. Additionally, to maintain a consistent flux of oxygen ions, the target current during sputtering was held at 0.5 μA.

The density functional theory (DFT) calculations presented in this work were performed using the generalized gradient approximation (GGA) of Perdew-Burke-Ernzerhof (PBE) for the exchange and correlation functional.[29] Projector augmented wave (PAW) potentials were used to take into account the effect of the ionic cores on the valence electrons .[30] All calculations were performed using the real-space grid GPAW code using periodic boundary conditions in the X and Y directions and free boundary conditions in the Z direction.[31,32] Pulay mixing of the density was used to improve the convergence and a low 0.01 eV Fermi-temperature was used throughout. We found that a grid spacing of 0.2 Å was enough to converge the adsorption energetics, and decreasing the grid spacing to 0.1 Å only changed the energetics by ~0.01 eV. For the calculations of chemisorbed O structures on unreconstructed Au(100), we employed a four layer $p(2 \times 2)$ surface slab, in which the lowest two layers were fixed to the calculated bulk crystal structure (with a lattice constant of a_0 = 4.168), while the remaining surface layers were allowed to fully

dx.doi.org/10.1021/jp3056653 | J. Phys. Chem. C 2012, 116, 18292−18299

optimize their geometry until the forces were less than 0.01 eV/Å. A 10 Å vacuum layer was found to be sufficient to ensure negligible coupling between periodic replicas of the slab. To model the hexagonal reconstruction of Au(100), we used a five layer (5 × 1) slab, previously employed in the literature, with a quasi-triangular reconstructed first layer containing six Au atoms arranged in an ABCCBA configuration.[33] This model covers all key features of the reconstruction, two-dimensional lateral contraction, rotation, and, qualitatively different buckled surface areas, giving a small net surface energy gain approximately in line with electrochemical experiments[34−36] and theoretical estimates.[37] To sample the Brillouin zone, 7 × 7 × 1 and 9 × 5 × 1 k-point meshes were used, for the $p(2 \times 2)$ and (5 × 1) cells, respectively, giving adsorption energies for oxygen converged to within 16 meV.[38]

Oxygen binding energies were defined as

$$E_b = (E_{O/Au} - E_{Au} - N_O E_{O_2}/2)/N_O \quad (1)$$

where N_O is the total number of oxygen atoms in the unit cell and $E_{O/Au}$, E_{Au}, and E_{O_2} are the total energies of the O/Au(100) system, of the clean Au(100) surface, and of the gas phase oxygen molecule, respectively. A negative value of the average adsorption energy indicates that the dissociative adsorption of O_2 is exothermic. A constant shift of −1.36 eV has been found between calculated and experimental oxygen binding energy values and was, hence, included in our calculated E_b values to match the experiment.[39]

RESULTS AND DISCUSSION

Figure 1 shows full and sectional O_2-TPDs of oxygen-sputtered Au(100) and STM images of the corresponding morphological changes due to the thermal desorption treatments. After sputtering Au(100) with O_2 (9.5×10^{15} ions/cm^2) at a sample temperature of 400 K, four oxygen desorption states arise, as evident from the desorption peaks seen in the full TPD in Figure 1A. These peaks resemble the $\gamma_1 - \gamma_4$ peaks in the O/Au(110) system previously described in the literature.[8] The maxima of the desorption peaks are 460, 550, 620, and 720 K and are labeled as γ_1, γ_2, γ_3, and γ_4, respectively. Rather than populating deep Au sites with oxygen as a result of sputtering at higher ion energies (≥1 keV), as observed in the case of Au(110),[8] it is seen in Figure 1A that the γ_1 and γ_2 low-temperature desorption states host the majority of the oxygen.

STM was used to investigate the surface morphology associated with the sectional TPDs and thermal treatments shown in Figure 1A. The as-sputtered Au(100) surface is seen in Figure 1B. The original step edges are still visible in the large-scale image of the modified surface, with pits up to 5−6 atomic layers deep, and the topmost layer of Au consists of small 2D islands, as seen in the inset of Figure 1B. It is important to note that, after sputtering, the well-known "hex" or $c(26 \times 48)$ reconstruction of Au(100) is lifted. The surface atoms of the hex-reconstructed clean Au(100) adopt hexagonal packing, whereas the bulk has a square lattice of atoms.[40−42] As a result, when the hex-reconstruction is lifted, the surface atoms undergo a transition from a hexagonal (or 3-fold) symmetric surface, to a square (or 4-fold) symmetric lattice. This surface restructuring carries a change in the high symmetry adsorption sites from 3- to 4-fold hollow sites. The adsorption of chemisorbed oxygen on Au substrates has been reported to lift the surface reconstructions on the (100),[16] (111),[11,16,27,43,44] and (110)[8,19] faces.

Annealing the O_2-sputtered Au(100) system to 485 K results in the full desorption of only the γ_1 oxygen phase, as seen in the "485 K" TPD in Figure 1A. STM images show that the surface morphology has changed significantly after this thermal treatment (Figure 1C) compared to the as-sputtered surface in Figure 1B. Most of the small islands have disappeared and the pits are now only one atomic layer deep. Further, the hex-reconstruction is present across the surface. Here, the reappearance of the hex-reconstruction after desorption of γ_1 suggests that the γ_1 oxygen phase could stabilize the unreconstructed surface by adsorbing on 4-fold hollow sites of the Au(100) square lattice, and DFT calculations below show further evidence of this claim. The clear difference between the morphology of the γ_1 and γ_2 phases indicates the presence of two types of oxygen present on the surface.

Oxygen adsorption has been found to favor hollow sites,[25,45,46] and therefore, the γ_1 phase is assigned to O chemisorbed in 4-fold hollows. This differs from the studies conducted on O/Au(110)-1 × 2, where the γ_1 state was assigned to a surface oxide, which was disputed after O/Au(111) studies, in which both γ_1 and γ_2 phases were assigned as oxygen species present on the surface.[8,26] Additionally, upon dissociating O_2 over a hot filament to induce chemisorbed atomic oxygen (and the lifting of the hex-reconstruction) on Au(100), one O_2 desorption peak was observed at 470 K,[16] in good agreement with the position of the γ_1 peak in Figure 1A, at 460 K. This supports our argument that γ_1 oxygen is chemisorbed oxygen rather than gold oxide.

Finally, bright protrusions, or "blisters", are seen in Figure 1C (indicated by white arrows), over which the hex-reconstruction continues unperturbed, indicating that they reside under the surface, potentially several layers down. These bright blisters are related to embedded oxygen, as we have implanted oxygen deep into the Au by sputtering and the bright blisters are not observed on clean Au(100).

To fully desorb the oxygen in the γ_2 state, the surface was further annealed to 570 K. The sectional O_2-TPD in Figure 1A labeled "570 K" shows γ_2 desorption, but no γ_1 desorption, indicating that oxygen did not diffuse from γ_2 to γ_1 and oxygen desorption ceased after the previous 485 K anneal. This supports the argument that γ_1 is related to the unreconstructed square Au surface. The complete healing of the surface is a kinetically limited process, and therefore, the morphology seen in Figure 1C represents a metastable state, with many pits one layer deep. Sputtering Au(111) with an inert gas such as neon or argon produces pits one layer deep that are stable up to 450 K,[20,21] similar to the structures observed in Figure 1C, which relax upon further annealing. After annealing to 570 K, oxygen from γ_1 and γ_2 states have desorbed, leaving only γ_3 and γ_4 phases behind, and the corresponding STM image is shown in Figure 1D. The terraces have healed and no longer contain pits. There are fewer domain boundaries between different orientations of the hex-reconstruction. The expanded view shows that, although the number of bright blisters (white arrows in Figure 1C,D) has decreased after the 570 K anneal, they have not completely disappeared. The Au surface has almost fully relaxed to the Au(100) reconstruction, in agreement with the return of long-range order on Au(110),[8] even in the presence of near surface (γ_3) and bulk (γ_4) oxygen. This clearly shows the reversibility of the Au morphology during oxygen adsorption and desorption.

Au(100) versus Au(111). The Au(100) surface undergoes a hex-reconstruction on top of the square bulk lattice, and we

dx.doi.org/10.1021/jp3056653 | J. Phys. Chem. C 2012, 116, 18292−18299

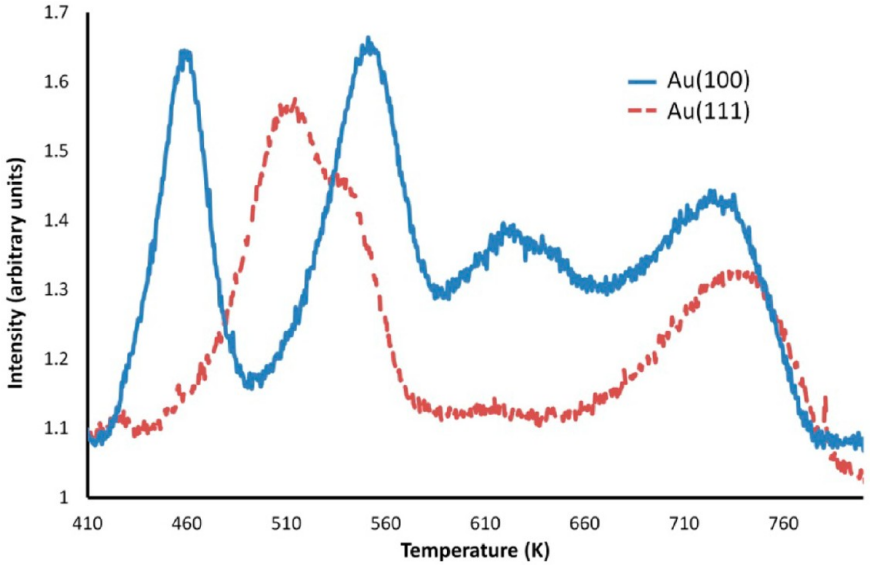

Figure 2. O_2 desorption following the same O_2-sputtering conditions (400 K, 9.5 × 10^{15} ions/cm^2) on Au(100) and Au(111).

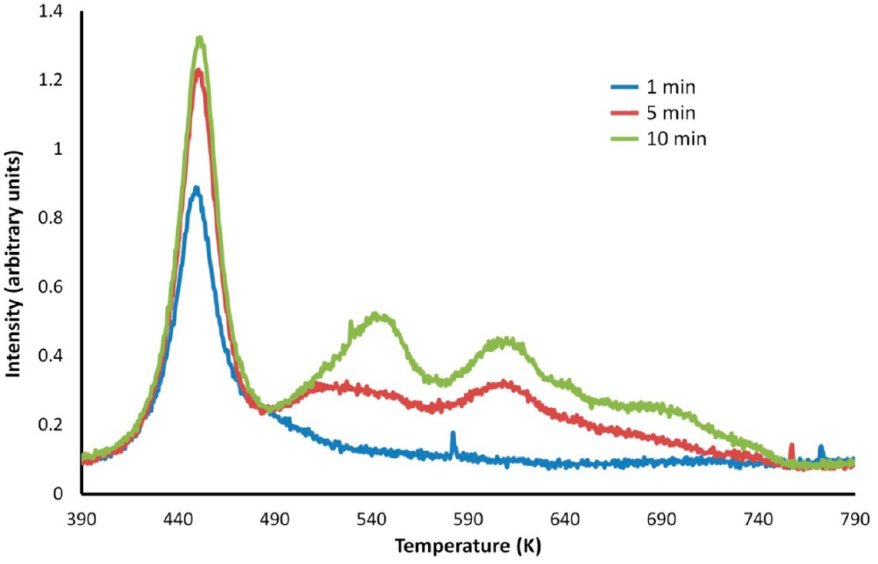

Figure 3. TPD spectra showing the dependence of O_2 sputter time on Au(100) at 320 K.

propose that the shift in morphology and adsorption site availability from the unreconstructed to the reconstructed surface accounts for the differences between the γ_1 and γ_2 desorption peaks. Investigating the difference between the oxygen phases on Au(100) and the phases found on Au(111), which has a compressed hexagonal reconstruction on top of a hexagonal lattice, will provide insight into the effect that the adsorption site may have on the state of oxygen.

Figure 2 shows TPD spectra following identical oxygen sputtering conditions (9.5 × 10^{15} ions/cm^2 at 400 K) for Au(111) and Au(100), resulting in very similar γ_4 peaks, where oxygen is buried deep into bulk Au. The lower temperature oxygen phases, which reside closer to the surface, differ by a larger degree between the two facets. There is no evidence of the low temperature γ_1 desorption peak from Au(111) in Figure 2, in line with our assignment of γ_1 as chemisorbed oxygen in 4-fold hollow sites, as only 3-fold hollow sites are present on the reconstructed and unreconstructed Au(111) surfaces. The low-temperature oxygen desorption peak from Au(111) is here assigned to γ_2 due to the significant overlap with the γ_2 desorption peak on Au(100). The γ_2 desorption peak has shifted to a lower temperature, indicating a lower desorption activation barrier on the reconstructed Au(111) surface than on the hex reconstructed surface of Au(100). Au(111) has two types of 3-fold hollow sites (hcp and fcc) which have a difference in O adsorption energy of ~0.2 eV.[45] We speculate that the γ_2 oxygen phase consists of two peaks due to atomic oxygen adsorbed in both hcp and fcc 3-fold hollow sites of the Au(111) surface.

The γ_3 peak is significantly suppressed, indicating either a larger desorption barrier of the bulk oxygen, due to the compressed Au(111) surface, or to the instability of oxygen to sit near the surface (i.e., it migrates to the surface or into the bulk). The γ_4 state has shifted to a slightly higher desorption T, again possibly due to the increased barrier for desorption due to the more compact Au(111) bulk lattice, which leads to a higher diffusion barrier of the oxygen toward the surface. It is important to note that under different O_2-sputtering conditions

dx.doi.org/10.1021/jp3056653 | J. Phys. Chem. C 2012, 116, 18292−18299

(5×10^{15} ions/cm^2, 200 K) on Au(111), Friend and co-workers observed a very small γ_1 peak (450 K) relative to the other states, as well as peaks at 580 K (γ_2), 625 K (γ_3), and 700 K (γ_4).[26] We suggest that the small γ_1 peak could arise from O adsorption on 4-fold hollow sites, as A-type steps on Au(111) exhibit 4-fold coordination, whereas B-type steps have 3-fold hollow coordination.[47]

Sputter Time Dependence. The oxygen phases in and on Au are affected by the number of incoming ions. By decreasing the flux of oxygen ions during implantation, the γ_1 species can be formed exclusively as seen in Figure 3. The desorption of O_2 was monitored after sputtering Au(100) at 320 K for different periods of time. After O_2-sputtering for 1 min (9.5×10^{14} ions/cm^2), one desorption peak (450 K) is observed, corresponding to the γ_1 state, which is preferentially populated with adsorbed oxygen. In contrast, after the electron-assisted dissociation of molecular oxygen on Au(110)-1 × 2, the γ_2 state was first occupied, and upon higher oxygen coverages, the γ_1 state was populated, perhaps after the induced lifting of the surface reconstruction at higher oxygen coverages. On the other hand, the O_2-sputtering preparation of atomic O induces surface atom diffusion due to the transfer of kinetic energy from the accelerated ions to the surface Au atoms, which aids the lifting of the hex-reconstruction, thereby preferentially yielding the γ_1 oxygen phase.

Upon increasing the sputtering time to 5 min (4.7×10^{15} ions/cm^2), three additional oxygen phases are seen, indicating that with long sputtering times the oxygen is implanted further into the Au. This trend is verified with a 10 min sputter (9.5×10^{15} ions/cm^2), which shows a larger ratio of deeper oxygen (higher temperature O_2 desorption peaks). The majority of the oxygen resides in the γ_1 phase on the surface after a 10 min sputter at 320 K, as seen in Figure 3, whereas the oxygen is more evenly distributed between the four phases after a 10 min sputter at 400 K (full TPD in Figure 1A). This result indicates that increasing the sample temperature to 400 K during the sputter enables deeper implantation of oxygen into the Au sample, due to an enhanced mobility of oxygen within the Au crystal. The desorption of O_2 resulting from chemisorbed O on Au surfaces has been reported in the literature to occur between 505 and 550 K on Au(111)[11,13,16,26,48] and 545−590 K on Au(110)-(1 × 2).[19,49] An additional state at lower temperatures (assigned as γ_1) is observed on the more open surfaces of Au(110) (415−490 K)[8,19] and here, Au(100) (460 K). We have assigned the γ_1 species as oxygen chemisorbed on 4-fold hollow sites on surface Au atoms in unreconstructed Au(100) islands and terraces, while γ_2 species are related to oxygen chemisorbed to undercoordinated Au atoms present in the reconstructed Au(100) surface.

The morphology of the 1 min sputtered surface at 320 K, which results solely in the γ_1 oxygen phase, is seen in Figure 4 and is smoother than the sputtered surface at higher temperatures and ion exposure (10 min sputter at 400 K) shown in Figure 1B. Small pits (1−2 atomic layers deep) and many small islands are seen on the surface, and the hex-reconstruction is lifted, as shown in Figure 4A. After annealing the surface to 400 K, the surface reconstruction partially returns, as seen in Figure 4B. It is clear from the TPD in Figure 3 that annealing to 400 K should not induce O_2 desorption, therefore the restructuring seen in Figure 4 is due to thermal relaxation. Based on our assignment of the γ_1 phase as chemisorbed oxygen on the unreconstructed surface, we suggest that the oxygen present on the surface (γ_1) resides in

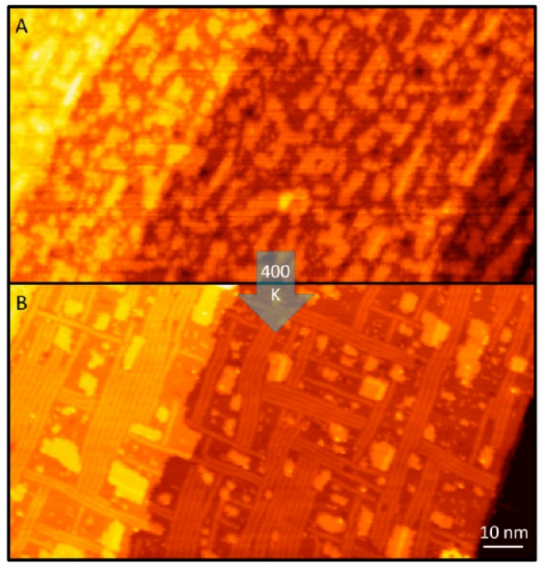

Figure 4. STM images of a Au(100) surface after O_2-sputtering for 1 min at 320 K, before and after a 400 K anneal. (A) As-sputtered surface before annealing. Scanning conditions: −0.4 V, 0.3 nA. (B) Post 400 K anneal (1.2 V, 0.6 nA).

the areas where the reconstruction is lifted on terraces and 2D islands. There is no evidence of bright blisters in the STM images in Figure 4 in which only γ_1 is present, and therefore oxygen is not deeply implanted into Au. Previous experiments of O/Au(111), where atomic O was adsorbed at 77 K and then annealed to room temperature, showed a decreased chemical activity for CO oxidation, explained by a stabilization of the metastable atomic oxygen species rather than a change in morphology.[50] Our results in Figure 3 show that the morphology of this system is dynamic and cannot be ruled out as a factor during reactivity studies.

Density Functional Theory Calculations. We performed DFT calculations to determine the nature of the different oxygen phases present in the experiments described above. Two different surface models, shown in Figure 5, were employed: a reconstructed Au(100) slab model (labeled as "RecAu(100)") which mimics the hex-reconstruction of clean Au(100), and an unreconstructed Au(100) slab (labeled as

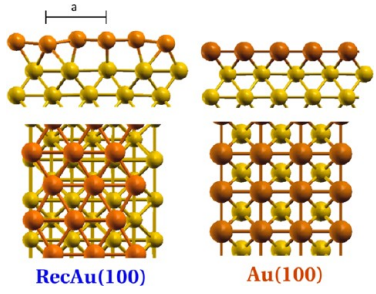

Figure 5. DFT optimized geometries of the reconstructed Au(100) and unreconstructed Au(100) surfaces [RecAu(100) and Au(100)]. The topmost Au layer is represented in a darker color in order to highlight the different periodicity between both surface unit cells. RecAu(100) represents a clean Au(100) surface that exhibits the hex-reconstruction, whereas Au(100) has a square lattice that is exposed when the reconstruction has been lifted. The scale bar (a) is 4.87 Å, showing the next nearest neighbor Au−Au spacing on RecAu(100).

dx.doi.org/10.1021/jp3056653 | J. Phys. Chem. C 2012, 116, 18292−18299

"Au(100)"), which has a square lattice representing the unreconstructed surface. This approach allows us to qualitatively describe the oxygen-induced morphological changes shown in Figures 1 and 4, because morphology likely plays a key role in determining the types of oxygen species present on the surface.

We consider the presence of both surface and subsurface oxygen species and Figure 6 displays the energy profile for the progressive depopulation, from right to left, of subsurface oxygen. Bottom and top panels in Figure 6 show a schematic representation of the relaxed oxygen-Au structures on the unreconstructed and reconstructed Au surfaces, respectively. Our results show that phases containing only subsurface oxygen ($2O_{sub}$, Figure 6) on both reconstructed and unreconstructed gold are highly unstable. Oxygen atoms reside in highly coordinated subsurface hollow sites in RecAu(100) with a binding energy of ~−0.6 eV [$2O_{sub}$/RecAu(100), Figure 6]. Subsurface oxygen atoms are 0.4 eV less stable in unreconstructed Au(100) than in RecAu(100) and bind to subsurface bridge sites [$2O_{sub}$/Au(100), Figure 6]. The inability of gold to stabilize subsurface oxygen is attributed to the chemical instability of bulk gold oxides.

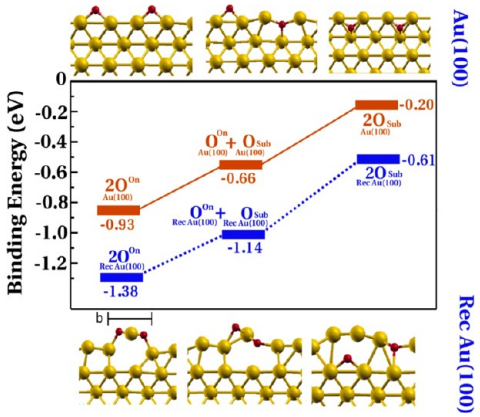

Figure 6. Energy profile and corresponding structures for the oxygen depopulation from subsurface to surface sites for unreconstructed and reconstructed Au(100) surfaces. The calculated adsorption binding energy of oxygen was referred to the gas phase molecule and the clean Au surfaces. The scale bar (b) is 4.93 Å, showing the next nearest neighbor Au−Au spacing on the oxygen-chemisorbed RecAu(100). Big yellow sphere, Au; small red sphere, O.

In contrast, the on-surface chemisorbed oxygen atoms are more stable by more than 0.7 eV for both RecAu(100) [$2O^{on}$/RecAu(100)] and Au(100) [$2O^{on}$/Au(100)], as seen in Figure 6. Therefore, the chemisorbed oxygen atoms on the surface are the primary species present in equilibrium conditions. Our results indicate that, with the presence of subsurface-implanted oxygen atoms, the structures easily convert to on-surface oxygen phases, promoting the release of gold atoms from the surface. As shown in Figure 6, undercoordinated Au atoms [$2O^{on}$/RecAu(100)] are highly effective at stabilizing the oxygen. The generation of the low coordinated Au adatom relieves surface tensile stress and yet the hex-reconstruction seems to be maintained in the presence of γ_2 oxygen (Figure 4B). DFT calculations show that the next nearest neighbor Au−Au spacing on RecAu(100), shown by the scale bar (a) in Figure 5, is 4.87 Å, and 4.93 Å on the O/RecAu(100), represented by scale bar (b) in Figure 6. This indicates a very small expansion of the surface lattice (~1%) when surface oxygen is incorporated into the hex-reconstruction of the Au(100) surface. Therefore, the oxygen species in $2O^{on}$/RecAu(100) (Figure 6) likely correspond to γ_2, whereas γ_1 is considered to be oxygen chemisorbed on the unreconstructed surface of Au(100) [$2O^{on}$/Au(100), Figure 6]. The difference in adsorption energy between $2O^{on}$/RecAu(100) and $2O^{on}$/Au(100) is 0.45 eV. This result is in good agreement with the 0.48 eV difference in the experimental desorption energies calculated for γ_1 and γ_2 from the TPD in Figure 1, following the Redhead approximation by Christmann et al., using their reported pre-exponential factors.[8,51]

When all of the γ_1 oxygen has been removed from the surface by annealing beyond its desorption temperature (Figure 1C), and the oxygen related or leading to the γ_2 phase is still present, the reconstruction has almost fully recovered as observed by STM imaging. This is in agreement with our DFT calculations, where the most stable structure for adsorbed oxygen on the hex-reconstructed Au(100) surface involves the incorporation of oxygen into the reconstruction, and the Au atoms are lifted and stabilized by O, but the spacing of reconstruction is maintained. These configurations, either $2O^{On}$/[RecAu(100)] or O^{On}/[RecAu(100)] + O_{Sub}/[RecAu(100)], are similar to the structures observed by molecular dynamic calculations of oxygen chemisorbed on uncoordinated Au atoms.[28] We argue that the γ_2 species ($2O^{On}$/[RecAu(100)]) is only present on the surface after annealing, promoting oxygen diffusion from the near surface into a more thermodynamically stable position. The diffusion of near surface oxygen to populate most of the γ_2 state occurs at temperatures very close to the γ_2 desorption temperature, meaning that the STM image of Figure 1C may contain little or no γ_2 oxygen.

CO Reactivity. The interaction of carbon monoxide (CO) with oxygen on Au(100) can help to distinguish which oxygen

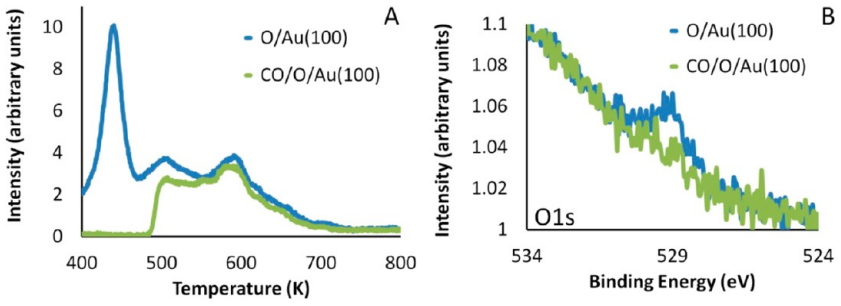

Figure 7. TPD and XPS showing the effect of 200 L CO exposure on O_2-sputtered Au(100). (A) TPD spectra of a 5 min O_2-sputter Au(100) surface before and after exposure to CO. (B) Corresponding O1s XPS before and after CO exposure of the oxygen-covered Au(100) surface.

dx.doi.org/10.1021/jp3056653 | J. Phys. Chem. C 2012, 116, 18292−18299

species are most reactive. The removal of oxygen after exposure to CO is seen in Figure 7 via TPD and XPS measurements. The oxygen that was present on the surface after O_2-sputtering at 320 K for 5 min corresponds to the O/Au(100) TPD in Figure 7A, in which the γ_1, γ_2, and γ_3 desorption peaks are observed. After exposure to 200 L of CO at 300 K, a subsequent TPD (CO/O/Au(100) in Figure 7A) shows that γ_1 is fully consumed. It has been shown previously that very large exposures of CO (8000 L) can reduce the amount of γ_1 and γ_2 oxygen from Au(110).[8] The third peak (γ_3) is unaffected by CO and therefore must be located deeper under the Au surface layer, in agreement with previous findings on different Au faces. Due to the calculated instability of subsurface oxygen, the inactivity of γ_3 oxygen to oxidize CO, and its insensitivity to XPS, we speculate that the γ_3 species is not located directly below the surface, as previously suggested, and is more likely near surface oxygen at least four layers deep.

Figure 7B shows the O1s region acquired by XPS before and after the CO exposure, where a small oxygen peak is present at 528.9 eV, but disappears after reacting with CO. It has previously been shown that atomic chemisorbed oxygen on Au(111) has a binding energy of 529.3 eV, whereas the Au oxide peak is present at 530.1 eV,[11,17,52] indicating that the oxygen signal detected in these experiments arises from atomic oxygen. In addition, during these experiments the XPS Au4f peaks were unaltered, in agreement with the observation of the more sensitive data related to the O1s peak, which establishes the formation of only chemisorbed oxygen but not gold oxide (Au_2O_3) during the oxygen-sputtering procedure reported here.[15,17,18] XPS results indicate that oxygen has been consumed after exposure to CO, in agreement with the O_2-sputtered Au(111) surface.[20] The disappearance of the first oxygen peak from the TPD in Figure 7A after exposure to CO indicates that the γ_1 phase is the most reactive and the only oxygen present on the surface after sputtering. We suggest that most of the γ_2 oxygen is not initially present on the surface, but annealing beyond the γ_1 desorption temperature allows oxygen to diffuse from the near surface to the now reconstructed surface to populate γ_2. Large morphological changes during extensive CO exposures at room temperature may also allow the release of near surface oxygen to populate the surface and be consumed, resulting in a decrease of the amount of oxygen that leads to γ_2 formation.

The reactivity of O/Au(100) for CO oxidation to CO_2 was also monitored by TPD, as shown in Figure 8. After O_2-sputtering, clean Au(100) at 300 K for 1 min, producing only the γ_1 phase, the sample was cooled to 90 K. CO (20 L) was adsorbed onto the cold O/Au sample which was then annealed to 500 K. In Figure 8, TPD spectra show that low-temperature CO_2 production is facilitated by the presence of surface oxygen on Au(100). The two peaks in the CO and CO_2 desorption (125 K, 170 K) arise from under-coordinated Au atoms on the Au surface and have previously been reported for surface sites on Au(110), where the number of under-coordinated adsorption sites is increased by sputtering, roughened Au surfaces as well as Au nanoparticles.[20,53,54] These results are in agreement with CO_2 production seen on O/Au(111), where the 125 K peak is due to step edge desorption, and the 170 K peak arises from Au atoms with lower coordination.[20]

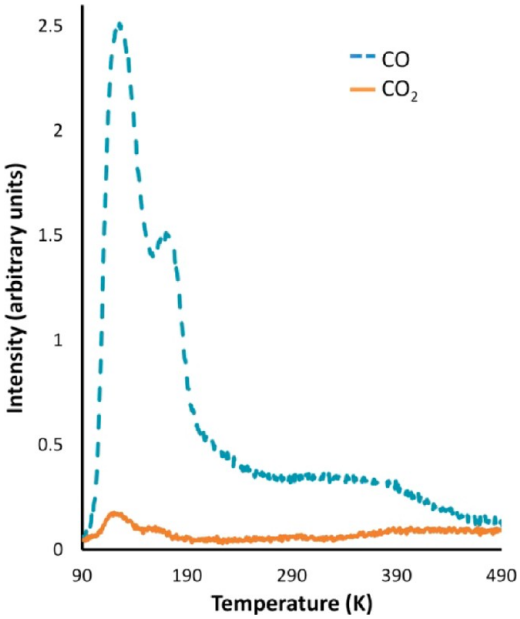

Figure 8. TPD spectra monitoring CO (dashed line) and CO_2 (solid line) desorption from O/Au(100).

CONCLUSIONS

Oxygen adsorption on Au(100) was achieved by means of oxygen-ion sputtering, where the resulting oxygen species were controlled by adjusting the substrate temperature, sputtering time and ion energy. Using combined STM, TPD, XPS, and DFT studies, we have elucidated the nature of the low-temperature desorption oxygen species (γ_1, γ_2) present on the surface of Au(100). We have assigned the γ_1 species as oxygen chemisorbed on 4-fold hollow sites on surface Au atoms in unreconstructed Au(100) islands and terraces, while γ_2 species are related to oxygen chemisorbed to undercoordinated Au atoms present in the reconstructed Au(100) surface. Most of the γ_2 oxygen forms via diffusion of near surface oxygen to the reconstructed Au(100) surface, which subsequently binds to undercoordinated Au during the annealing treatments during TPD experiments. Due to its inactivity toward adsorbed CO and its instability according to DFT calculations, we suggest that the γ_3 species is not located directly below the surface and is more likely near surface oxygen at least four layers deep, whereas γ_4 is assigned to bulk oxygen, in agreement with previous studies on Au(111) and Au(110). Sputtering with oxygen at higher substrate temperatures, or for longer periods of time, resulted in oxygen implanted deep into the Au in the γ_3 and γ_4 states. CO reactivity studies of O/Au(100) indicate that the γ_1 oxygen chemisorbed on unreconstructed Au(100) sites is the most reactive, reacting with CO to produce CO_2 at very low temperatures. We have shown the structural changes that accompany oxygen adsorption and desorption are representative of a highly dynamic system in which the morphology is strongly affected by the adsorbate.

AUTHOR INFORMATION

Corresponding Author

*E-mail: djs@bnl.gov.

Notes

The authors declare no competing financial interest.

ACKNOWLEDGMENTS

Experiments and calculations were carried out at the Center for Functional Nanomaterials at Brookhaven National Laboratory,

and the research was supported by the U.S. Department of Energy, Chemical Sciences Division, DE-AC02-98CH10886.

REFERENCES

(1) Haruta, M.; Yamada, N.; Kobayashi, T.; Iijima, S. *J. Catal.* **1989**, *115*, 301−309.
(2) Meyer, R.; Lemire, C.; Shaikhutdinov, S. K.; Freund, H. *Gold Bull.* **2004**, *37*, 72−124.
(3) Gong, J., *Chem. Rev.* **2012**, *112*, 2987-3054; 3055.
(4) Min, B. K.; Friend, C. M. *Chem. Rev.* **2007**, *107*, 2709−2724.
(5) Gong, J. L.; Mullins, C. B. *Acc. Chem. Res.* **2009**, *42*, 1063−1073.
(6) Outka, D. A.; Madix, R. J. *J. Am. Chem. Soc.* **1987**, *109*, 1708−1714.
(7) Xu, B. J.; Liu, X. Y.; Haubrich, J.; Friend, C. M. *Nat. Chem.* **2010**, *2*, 61−65.
(8) Gottfried, J. M.; Elghobashi, N.; Schroeder, S. L. M.; Christmann, K. *Surf. Sci.* **2003**, *523*, 89−102.
(9) Gottfried, J. M.; Schmidt, K. J.; Schroeder, S. L. M.; Christmann, K. *Surf. Sci.* **2003**, *525*, 197−206.
(10) Biener, M. M.; Biener, J.; Friend, C. M. *Surf. Sci.* **2005**, *590*, L259−L265.
(11) Saliba, N.; Parker, D. H.; Koel, B. E. *Surf. Sci.* **1998**, *410*, 270−282.
(12) Senanayake, S. D.; Stacchiola, D.; Liu, P.; Mullins, C. B.; Hrbek, J.; Rodriguez, J. A. *J. Phys. Chem. C* **2009**, *113*, 19536−19544.
(13) Wang, J.; Voss, M. R.; Busse, H.; Koel, B. E. *J. Phys. Chem. B* **1998**, *102*, 4693−4696.
(14) Ford, R. R.; Pritchard, J. *Chem. Commun. (London)* **1968**, 362−363.
(15) Canning, N. D. S.; Outka, D.; Madix, R. J. *Surf. Sci.* **1984**, *141*, 240−254.
(16) Davis, K. A.; Goodman, D. W. *J. Phys. Chem. B* **2000**, *104*, 8557−8562.
(17) Koslowski, B.; Boyen, H. G.; Wilderotter, C.; Kästle, G.; Ziemann, P.; Wahrenberg, R.; Oelhafen, P. *Surf. Sci.* **2001**, *475*, 1−10.
(18) Pireaux, J. J.; Chtaib, M.; Delrue, J. P.; Thiry, P. A.; Liehr, M.; Caudano, R. *Surf. Sci.* **1984**, *141*, 211−220.
(19) Gottfried, J. M.; Schmidt, K. J.; Schroeder, S. L. M.; Christmann, K. *Surf. Sci.* **2002**, *511*, 65−82.
(20) Biener, J.; Biener, M. M.; Nowitzki, T.; Hamza, A. V.; Friend, C. M.; Zielasek, V.; Bäumer, M. *ChemPhysChem* **2006**, *7*, 1906−1908.
(21) Hrbek, J.; Hoffmann, F. M.; Park, J. B.; Liu, P.; Stacchiola, D.; Hoo, Y. S.; Ma, S.; Nambu, A.; Rodriguez, J. A.; White, M. G. *J. Am. Chem. Soc.* **2008**, *130*, 17272−17273.
(22) Lopez, N.; Norskov, J. K. *J. Am. Chem. Soc.* **2002**, *124*, 11262−11263.
(23) Rodriguez, J. A.; Pérez, M.; Jirsak, T.; Evans, J.; Hrbek, J.; González, L. *Chem. Phys. Lett.* **2003**, *378*, 526−532.
(24) Baker, T. A.; Kaxiras, E.; Friend, C. M. *Top. Catal.* **2010**, *53*, 365−377.
(25) Baker, T. A.; Friend, C. M.; Kaxiras, E. *J. Phys. Chem. C* **2009**, *113*, 3232−3238.
(26) Zielasek, V.; Xu, B.; Liu, X.; Bäumer, M.; Friend, C. M. *J. Phys. Chem. C* **2009**, *113*, 8924−8929.
(27) Min, B. K.; Alemozafar, A. R.; Pinnaduwage, D.; Deng, X.; Friend, C. M. *J. Phys. Chem. B* **2006**, *110*, 19833−19838.
(28) Baker, T. A.; Friend, C. M.; Kaxiras, E. *J. Chem. Theory Comput.* **2009**, *6*, 279−287.
(29) Perdew, J. P.; Burke, K.; Ernzerhof, M. *Phys. Rev. Lett.* **1996**, *77*, 3865−3868.
(30) Blöchl, P. E. *Phys. Rev. B* **1994**, *50*, 17953−17979.
(31) Enkovaara, J.; Rostgaard, C.; Mortensen, J. J.; Chen, J.; Dulak, M.; et al. *J. Phys.: Condens. Matter* **2010**, *22*, 253202.
(32) Mortensen, J. J.; Hansen, L. B.; Jacobsen, K. W. *Phys. Rev. B* **2005**, *71*, 035109.
(33) Ercolessi, F.; Tosatti, E.; Parrinello, M. *Phys. Rev. Lett.* **1986**, *57*, 719−722.
(34) Feng, Y. J.; Bohnen, K. P.; Chan, C. T. *Phys. Rev. B* **2005**, *72*, 125401.
(35) Jacob, T. *Electrochim. Acta* **2007**, *52*, 2229−2235.
(36) Venkatachalam, S.; Kaghazchi, P.; Kibler, L. A.; Kolb, D. M.; Jacob, T. *Chem. Phys. Lett.* **2008**, *455*, 47−51.
(37) Havu, P.; Blum, V.; Havu, V.; Rinke, P.; Scheffler, M. *Phys. Rev. B* **2010**, *82*, 161418.
(38) Monkhorst, H. J.; Pack, J. D. *Phys. Rev. B* **1976**, *13*, 5188−5192.
(39) Wang, L.; Maxisch, T.; Ceder, G. *Phys. Rev. B* **2006**, *73*, 195107.
(40) Fedak, D. G.; Gjostein, N. A. *Surf. Sci.* **1967**, *8*, 77−97.
(41) Binnig, G. K.; Rohrer, H.; Gerber, C.; Stoll, E. *Surf. Sci.* **1984**, *144*, 321−335.
(42) Rodríguez de la Fuente, O.; González, M. A.; Rojo, J. M. *Phys. Rev. B* **2001**, *63*, 085420.
(43) Gibson, K. D.; Sibener, S. J. *J. Phys. Chem. A* **2007**, *111*, 12398−12401.
(44) Huang, L.; Chevrier, J.; Zeppenfeld, P.; Cosma, G. *Appl. Phys. Lett.* **1995**, *66*, 935−937.
(45) Daigle, A. D.; BelBruno, J. J. *Surf. Sci.* **2011**, *605*, 1313−1319.
(46) Jalili, S.; Zeini Isfahani, A.; Habibpour, R. *Comp. Theor. Chem.* **2012**, *989*, 18−26.
(47) Guo, Q.; Yin, F.; Palmer, R. E. *Small* **2005**, *1*, 76−79.
(48) Deng, X. Y.; Min, B. K.; Guloy, A.; Friend, C. M. *J. Am. Chem. Soc.* **2005**, *127*, 9267−9270.
(49) Sault, A. G.; Madix, R. J.; Campbell, C. T. *Surf. Sci.* **1986**, *169*, 347−356.
(50) Ojifinni, R. A.; Gong, J.; Flaherty, D. W.; Kim, T. S.; Mullins, C. B. *J. Phys. Chem. C* **2009**, *113*, 9820−9825.
(51) Redhead, P. A. *Vacuum* **1962**, *12*, 203−211.
(52) Krozer, A.; Rodahl, M. *J. Vac. Sci. Technol., A* **1997**, *15*, 1704−1709.
(53) Lemire, C.; Meyer, R.; Shaikhutdinov, S.; Freund, H. J. *Angew. Chem., Int. Ed.* **2004**, *43*, 118−121.
(54) Gottfried, J. M.; Schmidt, K. J.; Schroeder, S. L. M.; Christmann, K. *Surf. Sci.* **2003**, *536*, 206−224.